Thermo-Responsive Diblock Copolymers of Poly(*N*-isopropylacrylamide) and Poly(*N*-vinyl-2-pyrroridone) Synthesized via Organotellurium-Mediated Controlled Radical Polymerization (TERP)

Shin-ichi Yusa,*,† Shigeru Yamago,‡ Makoto Sugahara,† Sanae Morikawa,† Tohei Yamamoto,† and Yotaro Morishima§

Department of Materials Science and Chemistry, Graduate School of Engineering, University of Hyogo, 2167 Shosha, Himeji, Hyogo 671-2280, Japan, Institute for Chemical Research, Kyoto University, Uji, Kyoto 611-0011, Japan, and Department of Applied Physics and Chemistry, Graduate School of Engineering, Fukui University of Technology, 6-3-1 Gakuen, Fukui, Fukui 910-8505, Japan

Received March 31, 2007; Revised Manuscript Received June 5, 2007

ABSTRACT: Diblock copolymers of poly(*N*-isopropylacrylamide) (PNIPAM) and poly(*N*-vinyl-2-pyrrolidone) (PNVP) (PNIPAM$_m$-*b*-PNVP$_n$) with well-defined block lengths were successfully synthesized by organotellurium-mediated controlled radical polymerization (TERP) based on the finding that the homopolymerization of *N*-vinyl-2-pyrrolidone was better-controlled by TERP than by macromolecular architecture designed by interchange of xanthates (MADIX), TERP resulting in a narrower molecular weight distribution of PNVP. Heat-induced association properties in water of three block copolymers with different block lengths, PNIPAM$_{110}$-*b*-PNVP$_{53}$, PNIPAM$_{110}$-*b*-PNVP$_{234}$, and PNIPAM$_{76}$-*b*-PNVP$_{219}$, were characterized by ^{1}H NMR, turbidity, quasi-elastic light scattering (QELS), and static light scattering (SLS) techniques. All three block copolymers dissolve in water molecularly (as a unimer state) when the solution temperature is below an aggregation temperature (T_a) that is near a lower critical solution temperature (LCST) for the PNIPAM block. Comparing T_a between the two block copolymers of the same the PNIPAM block lengths (DP$_n$ = 110), the diblock copolymer with a shorter PNVP block length tend to associate at a lower temperature. On the other hand, the association occurred at a higher temperature for the diblock copolymers with shorter PNIPAM block lengths. When the temperature was raised above T_a, PNIPAM$_{110}$-*b*-PNVP$_{234}$ and PNIPAM$_{76}$-*b*-PNVP$_{219}$ formed apparently spherical core−corona micelles with aggregation numbers (N_{agg}) of 808 and 298, respectively at 60 °C. In contrast, PNIPAM$_{110}$-*b*-PNVP$_{53}$ formed a much larger aggregate with N_{agg} = 27 000. This aggregate was speculated to be a multi core aggregate formed by the association of individual core−corona micelles. The copolymers were found to be bound to gold nanoparticles in water through coordination interaction of the PNVP block with Au. The polymer coated gold nanoparticles indicated a temperature-dependent color change arising from a shift of the maximum wavelength of the plasomon band.

Introduction

It is known that controlled/"living" radical polymerization of nonconjugated monomers, such as vinyl acetate, *N*-vinylformamide (NVF), and *N*-vinyl-2-pyrrolidone (NVP), is difficult because their propagating radicals are so reactive that they have a tendency to undergo various side reactions during the polymerization. It has recently been reported that the controlled polymerization of NVF[1] and NVP[2,3] can be achieved by macromolecular architecture designed by interchange of xanthates (MADIX),[4] a kind of reversible addition−fragmentation chain transfer (RAFT)[5] controlled/"living" radical polymerization. It has also been reported that organotellium and organostibine provide effective promoters for highly controlled radical polymerization for a wide range of monomers including nonconjugated ones.[6−8] Proposed mechanisms for the organotellurium-mediated controlled radical polymerization (TERP) and MADIX are illustrated in Scheme 1. Conditions for these polymerizations are the same as conventional radical polymerization except for the addition of an organotellurium compound for TERP and xanthate for MADIX. Both mechanisms include a chain transfer between propagating radicals and chain transfer agents. Because the rate of the chain transfer is faster than that of the propagation, side reactions of the propagating radicals are prevented, and hence these polymerizations proceed in a living mechanism. A difference in the two polymerization mechanisms is that, in the case of MADIX, there is an "intermediate" whereas, in the case of TERP, there is a "transition state".[9−12]

Scheme 1

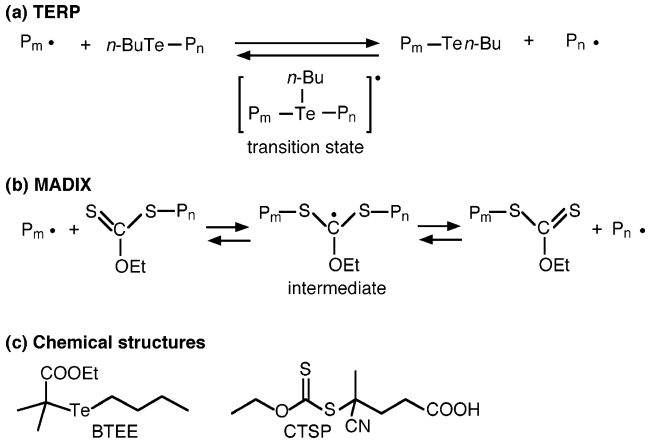

* Corresponding author. E-mail: yusa@eng.u-hyogo.ac.jp.
† University of Hyogo.
‡ Kyoto University.
§ Fukui University of Technology.

10.1021/ma070769x CCC: $37.00
Published on Web 07/10/2007

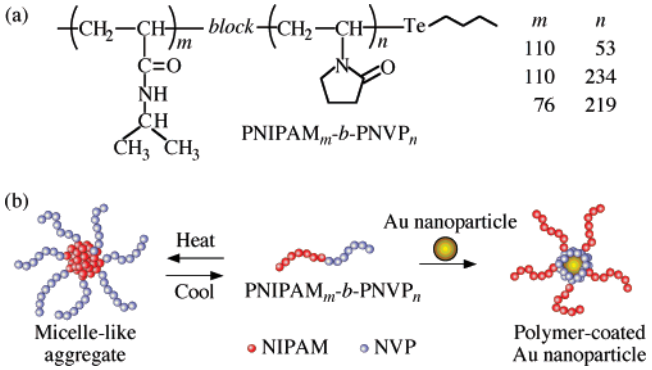

Figure 1. (a) Chemical structure of the diblock copolymer comprised of poly(*N*-isopropylacrylamide) and poly(*N*-vinyl-2-pyrrolidone) (PNIPAM$_m$-*b*-PNVP$_n$). (b) Schematic illustration of the micellization of PNIPAM$_m$-*b*-PNVP$_n$ as a function of temperature and the formation of polymer coated gold nanoparticle due to coordinated interaction between the PNVP block and gold nanoparticle.

Poly(*N*-vinyl-2-pyrrolidone) (PNVP) has been widely used in personal-care, agricultural, and many other industrial products because of its low toxicity and desirable performance.[13] PNVP is soluble in a large number of organic solvents, and it is also soluble in water due to hydrogen bonding between its pendent amide groups and water molecules. PNVP is a biocompatible material and thus used for various pharmaceutical applications.[14] Furthermore, PNVP shows a characteristic property of adhesion to various materials such as metals.[15,16]

Stimuli-responsive water-soluble polymer micelles formed by amphiphilic diblock copolymers are actively studied as a nano size vehicle for drug delivery systems and other purposes.[17] These amphiphilic diblock copolymers contain both a permanently hydrophilic block and a stimuli-responsive (i.e., "smart") block that undergoes a change from water-soluble to a water-insoluble state by physical and chemical external stimuli such as temperature, pH, and ionic strength. Thermoresponsive block copolymers that undergo micelle formation and dissociation depending on the temperature are particularly attractive materials because there is no need of any additive to the solution. Poly(*N*-isopropylacrylamide) (PNIPAM) shows a thermally reversible phase transition, i.e., a lower critical solution temperature (LCST), and it has been cited in the literature as a promising material for a number of biological applications including drug delivery systems.[18,19] There have been a number of reports dealing with PNIPAM containing thermoresponsive diblock copolymers.[20−22] However, to our best knowledge, there is no report on the synthesis and association behavior of diblock copolymers comprised of thermoresponsive PNIPAM block and biocompatible PNVP block (PNIPAM$_m$-*b*-PNVP$_n$) (Figure 1). PNIPAM$_m$-*b*-PNVP$_n$ is a good candidate for a thermoresponsive drug delivery vehicle because the diblock copolymer can form a micelle-like aggregate above LCST for the PNIPAM block with the biocompatible PNVP blocks forming an outer corona layer.

PNVP is known to stabilize gold nanoparticles due to multiple coordination of the pendent amide residues with the surface of gold nanoparticles.[23,24] Thus, gold nanoparticles may be effectively coated with the thermoresponsive diblock copolymer, NIPAM$_m$-*b*-PNVP$_n$, as schematically illustrated in Figure 1b, and each of the polymer coated gold nanoparticle may be separately dissolved in water when temperature is below LCST for the PNIPAM block. However, at high temperatures above LCST for the PNIPAM block, the gold nanoparticles may associate with each other due to the hydrophobic interactions between the dehydrated PNIPAM blocks. Visible absorption spectra of the surface plasmon band for gold nanoparticles are sensitive to the size of the gold nanoparticles. Well-dispersed gold nanoparticles indicate an absorption band around 520 nm with a pink color due to the surface plasmon resonance by the collective oscillation of electron density. The association of the gold nanoparticles induces a color change of the solution from pink to bluish-purple, which may be applied to colloidal sensors.[25−27]

In the present work, first, we compared two kinds of "living" radical polymerization techniques, i.e., TERP and MADIX, for the polymerization of NVP. Since we found molecular weight distributions for PNVP prepared by TERP were significantly narrower than those prepared by MADIX, we synthesized thermoresponsive diblock copolymers, PNIPAM$_m$-*b*-PNVP$_n$, by TERP. The thermoresponsive properties of the block copolymers were characterized using ^{1}H NMR, turbidity, and light scattering techniques. Furthermore, we found that gold nanoparticles were stabilized with NIPAM$_m$-*b*-PNVP$_n$ and that the polymer coated gold nanoparticles exhibited a color change due to their association and dissociation responding to a temperature change.

Experimental Section

Reagents. Ethyl-2-methyl-2-butyltelanilpropionate (BTEE) was obtained as a gift from Otsuka Chemical, which was stored in a Schlenk flask under Ar atmosphere until use.[28] 4-Cyano-4-((thioethoxy)sulfanyl)pentanoic acid (CTSP) was prepared according to the method reported by Zard and co-workers.[29] *N*-Isopropylacrylamide (NIPAM) (97%) from Aldrich was purified by recrystallization from a mixture of benzene and *n*-hexane (3/7, v/v). *N*-Vinyl-2-pyrroridone (NVP) (99.9%) was obtained as a gift from Nippon Shokubai and was dried over 4 Å molecular sieves and distilled under reduced pressure. 4,4'-Azobis(4-cyanopentanoic acid) (ACP, 98%) and 2,2'-azobis(isobutyronitrile) (AIBN, 98%), both from Wako Pure Chemical, were recrystallized from methanol. *N*,*N*-Dimethylformamide (DMF) was dried over 4 Å molecular sieves and distilled under reduced pressure. A gold nanoparticle aqueous solution (0.01%) was purchased from Funakoshi. The average hydrodynamic radius, $\langle R_h \rangle$, of the gold nanoparticle is 9.9 nm estimated by a quasi-elastic light scattering (QELS) measurement. Water was purified with a Millipore Milli-Q system. Other reagents were used as received.

Homopolymerization of NVP by TERP. NVP (11.1 g, 0.10 mol) and ACP (140 mg, 0.50 mmol) were mixed in a glass ampule with a magnetic stirring bar, and then the solution was degassed by purging with Ar gas for 30 min. BTEE (300 mg, 1.00 mmol) was added to the solution under Ar atmosphere. The molar ratio of [NVP]:[BTEE]:[ACP] was 100:1:0.5. The solution was heated at 60 °C for 3 h under Ar atmosphere. At different time intervals, a small portion of the polymerization mixture was sampled out using a syringe, and subjected to measurement of molecular weights by gel-permeation chromatography (GPC) and conversion by ^{1}H NMR.

Homopolymerization of NVP by MADIX. NVP (1.00 g, 9.00 mmol), ACP (5.05 mg, 0.018 mmol), and CTSP (22.3 mg, 0.09 mmol) were mixed in a glass ampule with a magnetic stirring bar, and the solution was heated at 60 °C for 195 min under Ar atmosphere. The [NVP]:[CTSP]:[ACP] molar ratio was 100:1:0.2. During the polymerization, samples were withdrawn periodically by a syringe to measure molecular weight by GPC and conversion by ^{1}H NMR.

Homopolymerization of NIPAM by TERP. NIPAM (2.26 g, 0.02 mol) and AIBN (82.1 mg, 0.50 mmol) were dissolved in 2.5 mL of DMF, and then the solution was degassed by purging with Ar gas for 30 min. BTEE (300 mg, 1.00 mmol) was added to the solution under Ar atmosphere. Polymerization was carried out at 60 °C for 3 h. During the polymerization, samples were withdrawn periodically by a syringe to measure molecular weight by GPC and conversion by ^{1}H NMR.

Block Copolymerization of NIPAM with NVP. A representative example for the preparation of the diblock copolymer of

NIPAM and NVP is as follows: NIPAM (3.00 g, 26.5 mmol) and AIBN (29.7 mg, 0.182 mmol) were dissolved in 3.2 mL of DMF. The solution was deoxygenated by purging with Ar gas for 30 min in a 25 mL three-necked round-bottom flask equipped with a rubber septum. To this flask, BTEE (72.3 mg, 0.241 mmol) was syringed through the septum under Ar atmosphere. Polymerization was carried out at 60 °C for 3 h. The reaction mixture containing NIPAM homopolymer (PNIPAM) was sampled out for ^{1}H NMR and GPC measurements. ^{1}H NMR and GPC results indicated that the conversion and number-average molecular weight (M_n) of the first block (PNIPAM) were >99% and 1.26×10^4 with a polydispersity (M_w/M_n) of 1.13, respectively. Then, the deoxygenated second monomer, NVP (13.4 g, 121 mol), and AIBN (9.93 mg, 0.0605 mmol) were introduced to the reaction mixture by a syringe. The second-stage polymerization at 60 °C was allowed to continue for 0.5 and 3.5 h before taking aliquot (~ 6 mL). ^{1}H NMR indicated that the conversions of NVP for 0.5 and 3.5 h were 18 and 70%, respectively. During the polymerization, samples were withdrawn periodically by a syringe to measure molecular weight by GPC and conversion by ^{1}H NMR. The polymers were purified by reprecipitating from chloroform into a large excess of diethyl ether twice. The polymers were dissolved in pure water and was recovered by a freeze-drying technique.

Preparation of PNIPAM$_{110}$-*b*-PNVP$_{53}$ Coated Gold Nano Particles. A mixture of PNIPAM$_{110}$-*b*-PNVP$_{53}$ and gold nanoparticles was kept at room temperature for 24 h in the dark to prevent light-induced flocculation.[30] This stock solution was diluted with an NaCl aqueous solution. The final concentrations of the diblock polymer, Au, and NaCl are 0.01 g/L, 0.005 wt % and 20 mM, respectively.

Measurements. GPC. GPC measurements were performed using a Tosoh RI8021 refractive index (RI) detector equipped with two Shodex LF-804 polystyrene mixed gel columns (bead size = 7 μm, pore size = 20−200 Å) working at 40 °C under a flow rate of 0.5 mL/min. A DMF solution containing 10-mM LiBr was used as eluent. The molecular weight and M_w/M_n of the polymer were calibrated with standard polystyrene samples.

^{1}H NMR. ^{1}H NMR spectra were obtained with a Bruker DRX-500 spectrometer operating at 500 MHz at various temperatures. Samples of the diblock copolymers were prepared as a 1.0 g/L D_2O solution. Chemical shifts were determined by using 3-(trimethylsilyl)propionic-2,2,3,3-d_4 acid sodium salt as an internal reference.

Percent Transmittance (% *T*). Values of % *T* for aqueous solutions of the diblock copolymers at a constant polymer concentration (C_p) of 1.0 g/L were measured with a JASCO V-530 spectrophotometer with a 1.0 cm path length quartz cell at various temperatures. The monitored wavelength was fixed at 600 nm. The temperature was changed from 25 to 60 °C with a heating rate of 0.5 °C/min with a JASCO ETC-505T thermostat system.

Light Scattering. QELS data were obtained with an Otsuka Electronics Photal DLS-7000HL light scattering spectrometer equipped with an ALV5000/EPP multi-τ digital time correlator. A He−Ne laser (10.0 mW at 632.8 nm) was used as a light source. Sample solutions for QELS measurements were filtered with a 0.2 μm pore size membrane filter. To obtain the relaxation time distribution, $\tau A(\tau)$, the inverse Laplace transform (ILT) analysis was performed using the algorithm REPES.[31−33] The average translational diffusion coefficient ($\langle D \rangle$) is calculated from $\langle D \rangle = \langle \Gamma \rangle / q^2$, where $\langle \Gamma \rangle$ is the inverse of $\langle \tau \rangle$, i.e., the average relaxation rate, and $q = (4\pi n/\lambda) \sin(\theta/2)$ with n being the refractive index of solvent, λ being the wavelength (=632.8 nm), and θ being the scattering angle. The symbol "$\langle\rangle$" means an average value. $\langle R_h \rangle$ is calculated using the Einstein−Stokes relation $\langle R_h \rangle = k_B T / 6\pi\eta\langle D \rangle$, where k_B is Boltzmann's constant, T is the absolute temperature, and η is the solvent viscosity.

Static light scattering (SLS) measurements were performed on an Otsuka Electronics Photal DLS-7000HL light scattering spectrometer with a He−Ne laser (10.0 mW at 632.8 nm) at a constant C_p of 1.0 g/L at 60 °C. The angular dependence of the excess absolute scattering intensity, the Rayleigh ratio ($R_{vv}(\theta)$) of a dilute dispersion can lead to weight-average molecular weight (M_w) and

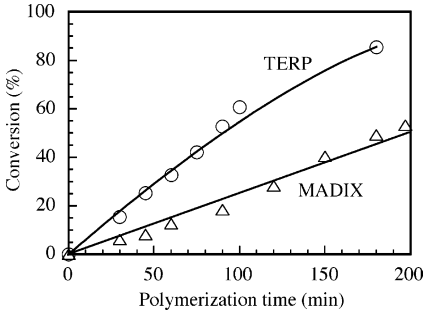

Figure 2. Time−conversion plots for bulk polymerization of NVP by TERP (○) and MADIX (△) at 60 °C. The molar ratio of [NVP]:[BTEE]:[ACP] and [NVP]:[CTSP]:[ACP] were 100:1:0.5 and 100:1:0.2, respectively.

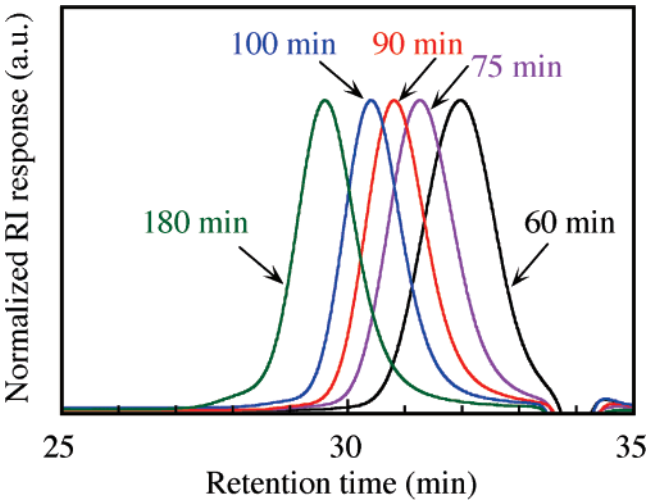

Figure 3. Evolution of normalized GPC elution profiles with time during the polymerization of PNVP by TERP.

z-average radius of gyration ($\langle R_g \rangle$) of scattering objects.[34,35] Values of dn/dC_p were determined with an Otsuka Electronics Photal DRM-1020 differential refractometer at 60 °C.

Results and Discussion

Comparison of TERP and MADIX in the Polymerization of NPV. Bulk polymerizations of NVP by TERP and MADIX controlled radical polymerization techniques were compared at 60 °C under Ar atmosphere using known amounts of BTEE and CTSP (Scheme 1) for TERP and MADIX, respectively. In the case of TERP, ca. 90% conversion was attained 3 h after the polymerization was started, whereas only ca. 45% conversion was reached with MADIX (Figure 2). The polymerization rate is about twice faster for TERP than that for MADIX, presumably because [CTSP]/[initiator] and [BTEE]/[initiator] are 5 and 2, respectively. When the [CTSP]/[initiator] ratio decreases <5, i.e., a higher initiator concentration, M_w/M_n of PNVP is remarkably broad.

Figure 3 shows normalized GPC elution profiles demonstrating evolution of molecular weight during bulk polymerization of NVP by TERP. The molecular weight of the polymer increases progressively with polymerization time. These GPC elution profiles are unimodal and symmetrical with no indication of the presence of uncontrolled polymers.

In Figure 4, M_n and M_w/M_n values for PNVP obtained by TERP and MADIX are plotted as a function of the monomer conversion. The M_n values for PNVP prepared by TERP and MADIX increase almost linearly with the conversion. All values of M_n are close to theoretical values predicted for a "living" mechanism. The values of M_w/M_n for MADIX are in the range

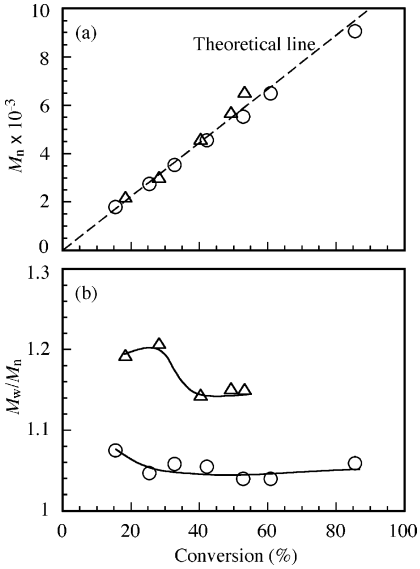

Figure 4. Dependence of M_n (a) and M_w/M_n (b) on monomer conversion in the bulk polymerization of NVP at 60 °C by TERP (○) and MADIX (△). The broken line represents the theoretical line.

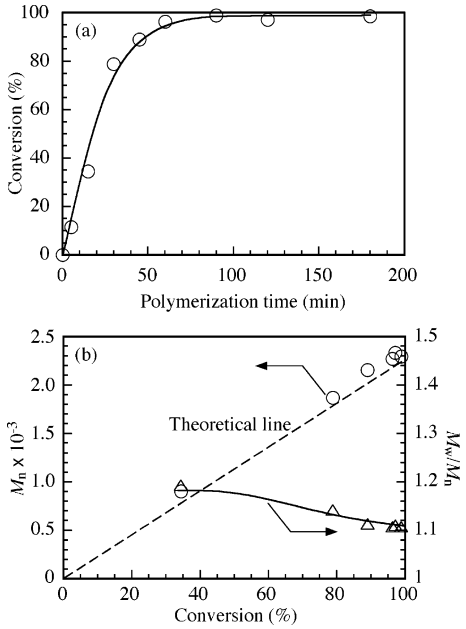

Figure 5. (a) Time−conversion plots for the polymerization of NIPAM by TERP. (b) Dependence of M_n (○) and M_w/M_n (△) on monomer conversion in the polymerization of NIPAM at 60 °C by TERP. The broken line represents the theoretical line.

of 1.1−1.2. On the other hand, the values of M_w/M_n for TERP are in a somewhat narrower range of 1.0−1.1, nearly independent of the conversion. These observations indicate that the polymerizations of NVP by TERP and MADIX are well controlled, proceeding in a "living" mechanism. It is to be noted, however, that there is a subtle difference between the two polymerization techniques, TERP resulting in a narrower molecular weight distribution of PNVP (see Supporting Information).

Synthesis of PNIPAM$_m$-*b*-PNVP$_n$ by TERP. Having confirmed that the TERP method allows for a better controlled polymerization of NVP resulting in a narrower molecular weight distribution, we applied the TERP method to the synthesis of diblock copolymers of PNIPAM and PNVP.

First, we performed solution polymerization of NIPAM in DMF at 60 °C by TERP. At different time intervals, a small

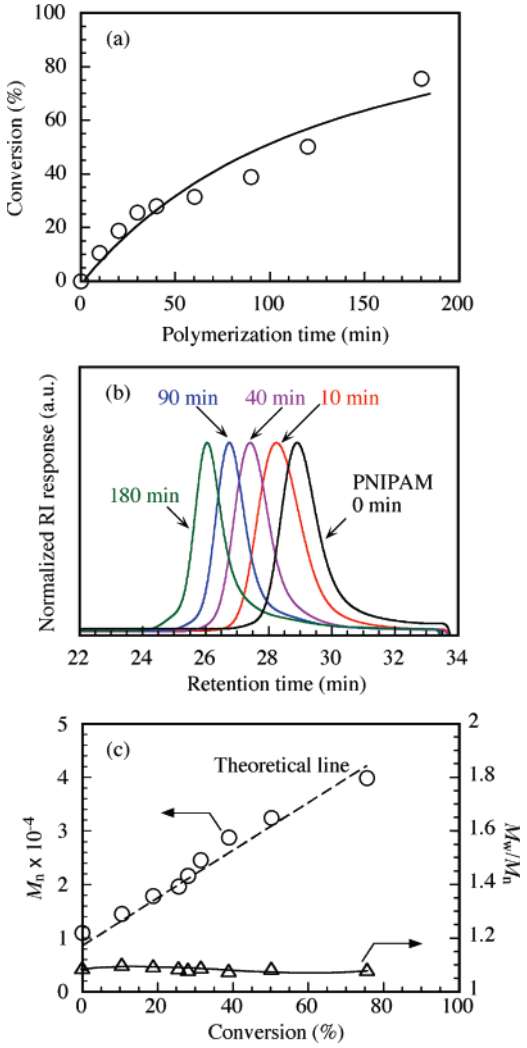

Figure 6. (a) Time−conversion plots for block copolymerization of NVP in the presence of the PNIPAM macropromoter in DMF at 60 °C by TERP. (b) Normalized GPC elution profiles with time during the synthesis of PNIPAM$_m$-*b*-PNVP$_n$ diblock copolymer. (c) Dependence of M_n (○) and M_w/M_n (△) on monomer conversion in the block copolymerization of NVP in the presence of the PNIPAM macropromoter at 60 °C by TERP. The broken line represents the theoretical line.

portion of the polymerization mixture was sampled out with a syringe and subjected to measurement of molecular weight by GPC and conversion by ^{1}H NMR. Figure 5a shows time−conversion plots for solution polymerization of NIPAM. After 2 h, a monomer conversion of ca. 100% is reached. Figure 5b shows conversion−M_n and conversion−M_w/M_n plots. M_n for NIPAM by TERP increases linearly with increasing conversion. All values of M_n are close to the theoretical values predicted for a living mechanism. The values of M_w/M_n are reasonably small, suggesting that the polymerization of NIPAM by TERP progressed in accordance with a controlled/"living" mechanism. The polymerization rate is fast, and a nearly complete conversion of NIPAM is reached only in 3 h.

Next, we applied the TERP technique to one pot synthesis of diblock copolymers of PNIPAM and PNVP. NIPAM was polymerized for 3 h, followed by the addition of NVP to the polymerization mixture of NIPAM. Figure 6a shows the time−conversion profile for the block copolymerization of NVP by TERP in the presence of a PNIPAM macropromoter. After 3 h, the monomer conversion reached ca. 80%. A time evolution of normalized GPC elution profiles observed during the block

Table 1. Compositions and Molecular Weights of the Polymers

sample code	conversion[a] (%)	DP_n PNIPAM[b]	DP_n PNVP[c]	M_n[c] (NMR) × 10^{-4}	M_n[d] (GPC) × 10^{-4}	M_w/M_n[d]
$PNIPAM_{110}$	>99	110		1.24	1.26	1.13
$PNIPAM_{76}$	95	76		0.86	1.09	1.09
$PNIPAM_{110}$-*b*-$PNVP_{53}$	18	110	53	1.83	1.70	1.09
$PNIPAM_{110}$-*b*-$PNVP_{234}$	70	110	234	3.85	2.63	1.11
$PNIPAM_{76}$-*b*-$PNVP_{219}$	76	76	219	3.29	3.67	1.15

[a] The polymerization mixture was extracted and determined by ^{1}H NMR. [b] Estimated from the conversion determined by ^{1}H NMR and the initial ratio of NIPAM to BTEE. [c] Estimated by ^{1}H NMR for the purified diblock copolymers. [d] Estimated by GPC eluted with a DMF solution containing a 10-mM LiBr.

copolymerization of NVP in the presence of the PNIPAM macropromoter is shown in Figure 6b. The molecular weight of the diblock copolymer increases progressively with polymerization time. These GPC elusion profiles are unimodal suggesting no side reactions. Figure 6c shows M_n and M_w/M_n estimated from GPC measurement for the block copolymers of PNIPAM and PNVP as a function of the monomer conversion during the polymerization of NVP in the presence of the PNIPAM macropromoter. M_n increases almost linearly with the conversion. All values of M_n are close to the theoretical values predicted for a "living" mechanism. The values of M_w/M_n are nearly constant at ca. 1.1 independent of the conversion. These observations indicate that the block copolymerization of NVP is well controlled. Thus, we were able to obtain diblock copolymers of PNIPAM and PNVP of different PNIPAM and PNVP block lengths with well-controlled block lengths. The number-average degrees of polymerization (DP_n) of the PNIPAM and PNVP blocks were estimated form GPC and ^{1}H NMR as listed in Table 1. Three samples with different block lengths are denoted as $PNIPAM_{110}$-*b*-$PNVP_{53}$, $PNIPAM_{110}$-*b*-$PNVP_{234}$, and $PNIPAM_{76}$-*b*-$PNVP_{219}$. The molecular weight distribution is narrow with M_w/M_n values ranging from 1.09 to 1.15 as estimated from GPC data.

Thermo-Responsive Properties of the Block Copolymers. It is known that PNIPAM shows an LCST of ca. 32 °C, i.e., PNIPAM dissolves in water at temperatures below LCST but it precipitates above LCST. Therefore, the diblock copolymer of PNIPAM and PNVP is expected to behave as a thermoresponsive polymer. Both the PNIPAM and PNVP blocks are soluble in water at room temperature, whereas the polymers may associate into a micelle-like aggregate at temperatures above LCST for the PNIPAM block, the dehydrated PNIPAM blocks forming a core and hydrophilic PNVP blocks forming coronas.

Heat-induced association of AB diblock copolymers comprised of hydrophilic and PNIPAM blocks can be observed by ^{1}H NMR spectroscopy.[21,22] Figure 7 compares ^{1}H NMR spectra for $PNIPAM_{110}$-*b*-$PNVP_{234}$ in D_2O at 25 and 60°C. The resonance band at 1.5−2.6 ppm is attributed to the sum of the main chain protons and pendent methylene protons of PNVP. The broad resonance band centered at 3.3 ppm can be assigned as the pendent methylene protons "*e*" in PNVP. The resonance bands at 1.2 and 3.9 ppm are attributed to the methyl "*a*" and methine protons "*g*" in the pendent isopropyl group in PNIPAM. The resonance peaks at 1.5−2.6 and 3.3 ppm due to PNVP at 60 °C are slightly larger than those at 25 °C, suggesting that the motions of the PNVP blocks increase with increasing temperature. On the other hand, the resonance peak intensity around 1.2 ppm, that is "*a*" due to the NIPAM pendent methyl protons, at 60 °C is markedly lower than that at 25 °C, indicating that motions of the PNIPAM blocks are highly restricted at 60°C.

The normalized NMR peak intensity ratios ($I_{1.2}/I_{3.3}$) for the PNIPAM pendent methyl proton at 1.2 ppm and the PNVP

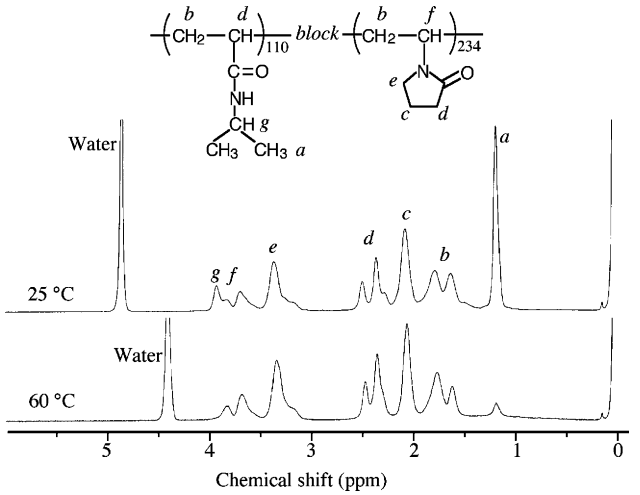

Figure 7. Comparison of ^{1}H NMR spectra for $PNIPAM_{110}$-*b*-$PNVP_{234}$ at C_p = 1.0 g/L in D_2O at 25 and 60 °C.

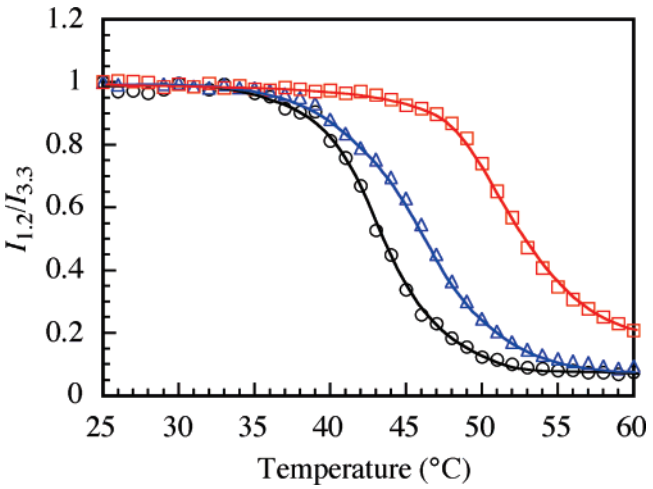

Figure 8. Plots of normalized NMR signal intensity ratio of $I_{1.2}/I_{3.3}$ for $PNIPAM_{110}$-*b*-$PNVP_{53}$ (○), $PNIPAM_{110}$-*b*-$PNVP_{234}$ (△), and $PNIPAM_{76}$-*b*-$PNVP_{219}$ (□) at C_p = 1.0 g/L in D_2O as a function of temperature, where $I_{1.2}$ and $I_{3.3}$ are NMR signal intensities at 1.2 and 3.3 ppm, respectively.

methylene protons at 3.3 ppm were measured at varying temperatures. In Figure 8, the $I_{1.2}/I_{3.3}$ ratios for the diblock copolymers at C_p = 1.0 g/L in D_2O are plotted as a function of temperature. The $I_{1.2}/I_{3.3}$ ratios are normalized with the $I_{1.2}/I_{3.3}$ value at 25°C. The normalized $I_{1.2}/I_{3.3}$ ratio for $PNIPAM_{110}$-*b*-$PNVP_{234}$ is practically constant at temperatures below 40 °C, however the $I_{1.2}/I_{3.3}$ ratio starts to decrease with increasing temperature from 40 to 55 °C. The decrease in $I_{1.2}/I_{3.3}$ above 40°C is due to a restricted motion of the PNIPAM blocks as a result of the formation of a hydrophobic microdomain. The temperature for the onset of a decrease in $I_{1.2}/I_{3.3}$ for the diblock copolymer with the shorter PNIPAM block length, $PNIPAM_{76}$-*b*-$PNVP_{219}$, is higher than those for the block copolymers with

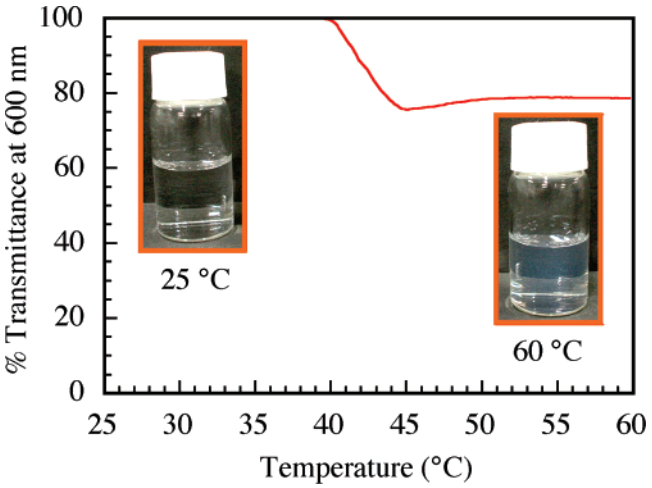

Figure 9. Percent transmittance (% *T*) at 600 nm for an aqueous solution of PNIPAM$_{110}$-*b*-PNVP$_{234}$ at C_p = 1.0 g/L as a function of temperature. The temperature was changed with a heating rate of 0.5 °C/min. Inserts show digital photographs for aqueous solution of PNIPAM$_{110}$-*b*-PNVP$_{234}$ at 25 °C and 60 °C.

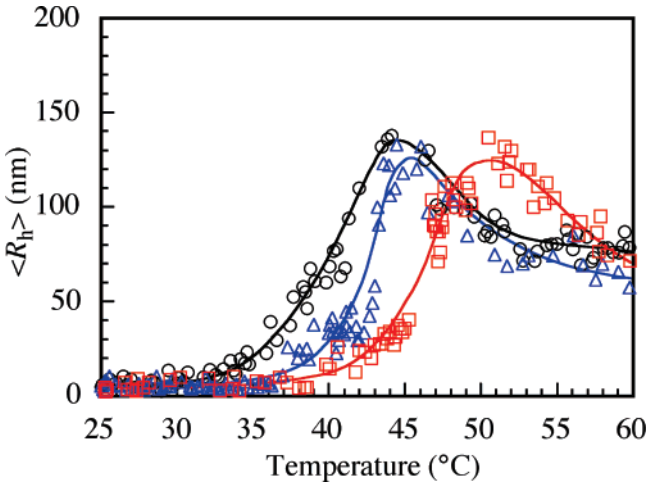

Figure 10. Intensity-average hydrodynamic radius ($\langle R_h \rangle$) for PNIPAM$_{110}$-*b*-PNVP$_{53}$ (○), PNIPAM$_{110}$-*b*-PNVP$_{234}$ (△), and PNIPAM$_{76}$-*b*-PNVP$_{219}$ (□) at C_p = 1.0 g/L in water as a function of temperature.

longer PNIPAM block lengths. This observation suggests that the association occurs at a higher temperature for the diblock copolymers with shorter PNIPAM block lengths. In the case of the same PNIPAM block lengths (DP$_n$ = 110), the diblock copolymers with shorter PNVP block lengths tend to associate at lower temperatures.

The diblock copolymers in aqueous solutions undergo a transition from a molecularly dissolved unimer state at low temperatures to an association state above an aggregation temperature (T_a). As shown in Figure 9, values of % *T* monitored at 600 nm for an aqueous solution of PNIPAM$_{110}$-*b*-PNVP$_{234}$ at C_p = 1.0 g/L are 100% below 40 °C, and the solution shows no Tyndall scattering. The % *T* value decreases with increasing temperature, reaching a smaller value of 75% above 45 °C. The Tyndall scattering at 60 °C, characteristic of a colloidal solution, was visually confirmed. The turbid solution above T_a became clear again when the solution was cooled below T_a. The T_a values for the diblock copolymers were estimated from a break in the % *T* vs temperature plot. The T_a values for PNIPAM$_{110}$-*b*-PNVP$_{53}$, PNIPAM$_{110}$-*b*-PNVP$_{234}$, and PNIPAM$_{76}$-*b*-PNVP$_{219}$ are thus estimated to be 38.5, 40.6, and 44.0 °C, respectively (Table 2). Comparing the block copolymers of the same PNIPAM block lengths (i.e., PNIPAM$_{110}$), T_a is higher for longer PNVP block length. Furthermore, comparing the block copolylmers of similar PNVP block lengths (i.e., PNVP$_{234}$ and PNVP$_{219}$), T_a is higher for shorter PNIPAM block length. These observations are consistent with the aforementioned observations in ^{1}H NMR spectra. McCormick et al.[21] reported the thermoresponsive micellization in water of poly(*N*,*N*-dimethylacrylamide)-*block*-poly(*N*-isopropylacrylamide) (PDMA-*b*-PNIPAM) with different block lengths. Our results are consistent with their findings that the association temperature for PDMA-*b*-PNIPAM increases with decreasing the PNIPAM block length.

Characterization of Micelle-like Aggregates of the Block Copolymers above T_a. The association behavior of PNIPAM$_m$-*b*-PNVP$_n$ in water above T_a was characterized using a QELS method (see Supporting Information). Below 30 °C, the block copolymers dissolve molecularly in water (i.e., in the unimer state) with $\langle R_h \rangle$ values on the order of ca. 10 nm (Figure 10). When the temperature is increased, the $\langle R_h \rangle$ value starts to increase around T_a, reaching a maximum $\langle R_h \rangle$ value ranging 130−140 nm and then decreases down to 70−80 nm with a further increase in temperature.

Shown in Figure 11a are representative examples of relaxation time distributions for PNIPAM$_{76}$-*b*-PNVP$_{219}$ at 60 °C in water at different polymer concentrations. The polymer at 60 °C exhibits a unimodal distribution, and $\langle R_h \rangle$ values for PNIPAM$_{76}$-*b*-PNVP$_{219}$ are estimated to be 112, 82.8, and 70.8 nm at C_p = 2.0, 1.0, and 0.4 g/L, respectively. In Figure 11b, the $\langle R_h \rangle$ values for the polymer aggregates formed from the diblock copolymers are plotted against the polymer concentration. These observations suggest that the polymer aggregates at 60 °C are a core−corona type polymer micelle, as one can reasonably anticipate from the chemical structure of the block copolymers. As indicated by the set of QELS data, the hydrodynamic size of the polymer micelle depends on the polymer concentration for all the three block copolymers, $\langle R_h \rangle$ increasing with increasing C_p. These observations suggest that the aggregation number (N_{agg}) of the polymer micelle (the number of polymer chains forming one micelle) increases with increasing C_p. It should be reasonable to assume that above T_a the diblock copolymers form spherical core−corona micelles with a hydrophobic core formed by aggregation of dehydrated PNIPAM blocks and a corona formed by permanently water-soluble PNVP blocks. From the temperature dependence of the $\langle R_h \rangle$ value shown in Figure 10, the dehydration of the PNIPAM blocks seems to occur progressively over a range of temperatures. The micelle size increases as the dehydration proceeds. However, after reaching a maxi-

Table 2. Quasi-Elastic and Static Light Scattering Data for the Micelle-Like Aggregate Formed from the Diblock Copolymers at 60 °C and T_a

sample code	$\langle R_h \rangle^a$ (nm)	$\langle R_g \rangle^a$ (nm)	$\langle R_g \rangle / \langle R_h \rangle$	$M_w{}^a \times 10^{-7}$	$N_{agg}{}^b$	$dn/dC_p{}^c$ (mL/g)	$T_a{}^d$ (°C)
PNIPAM$_{110}$-*b*-PNVP$_{53}$	86.9	243	2.7	50.1	27 000	0.15	38.5
PNIPAM$_{110}$-*b*-PNVP$_{234}$	69.8	55.3	0.79	2.36	808	0.15	40.6
PNIPAM$_{76}$-*b*-PNVP$_{219}$	82.8	77.6	0.94	1.26	298	0.14	44.0

[a] Estimated by QELS and SLS in water at 60 °C, where C_p is fixed at 1.0 g/L. [b] Aggregation numbers at 60 °C estimated from M_w of the aggregates determined by SLS and M_w of the corresponding unimers determined by GPC. [c] Estimated with the differential refractometer at 60 °C. [d] Association temperature (T_a) in water determined by % transmittance at 600 nm.

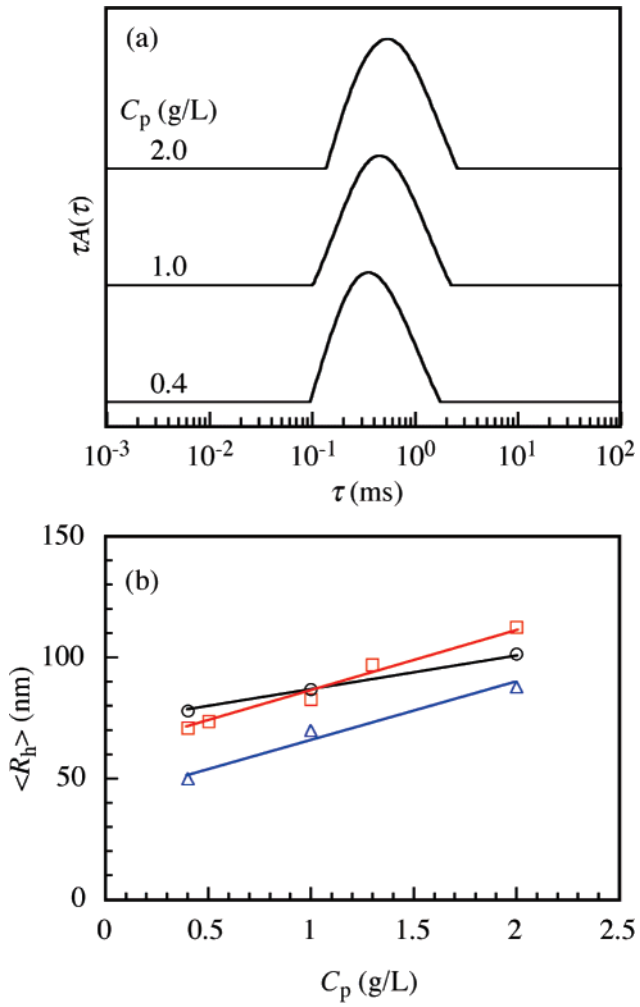

Figure 11. (a) Typical examples of QELS relaxation time distributions for PNIPAM$_{76}$-*b*-PNVP$_{219}$ at C_p = 2.0, 1.0, and 0.4 g/L in water at 60 °C. (b) Concentration dependence of intensity-average hydrodynamic radius ($\langle R_h \rangle$) for PNIPAM$_{110}$-*b*-PNVP$_{53}$ (○), PNIPAM$_{110}$-*b*-PNVP$_{234}$ (△), and PNIPAM$_{76}$-*b*-PNVP$_{219}$ (□) in water at 60 °C.

mum size, the micelle decreases in size probably because the micelle core becomes more compact as a result of further dehydration of the PNIPAM blocks with a further increase in temperature (Figure 10).

Figure 12 exhibits the angular dependence of the excess Rayleigh ratio for the three block copolymers measured at 60 °C at a fixed polymer concentration of 1.0 g/L. From the intercept and the slope of the plots, we estimated values of M_w and $\langle R_g \rangle$. Since $\langle R_h \rangle$ of the polymer micelle depends on the polymer concentration, the M_w and $\langle R_g \rangle$ values thus estimated are only apparent values at a fixed polymer concentration of 1.0 g/L. Values of $\langle R_h \rangle$, $\langle R_g \rangle$, and M_w estimated from light scattering data at 60 °C are summarized in Table 2. The value of N_{agg} listed in Table 2 was calculated from the ratio of M_w estimated by SLS for the micelle at 60 °C at a fixed C_p of 1.0 g/L and M_w estimated by GPC for the unimer state. The N_{agg} values for PNIPAM$_{110}$-*b*-PNVP$_{234}$ and PNIPAM$_{76}$-*b*-PNVP$_{219}$ were calculated to be 808 and 298, respectively; the micelle size of PNIPAM$_{110}$-*b*-PNVP$_{234}$ is smaller than that of PNIPAM$_{76}$-*b*-PNVP$_{219}$ (Table 2). This observation suggests that longer PNIPAM blocks tend to form a micelle core with a larger N_{agg} because the longer PNIPAM block is more hydrophobic at temperatures above T_a. The N_{agg} value for PNIPAM$_{110}$-*b*-PNVP$_{53}$ was found to be 27,000, which is much larger than those for PNIPAM$_{110}$-*b*-PNVP$_{234}$ and PNIPAM$_{76}$-*b*-PNVP$_{219}$.

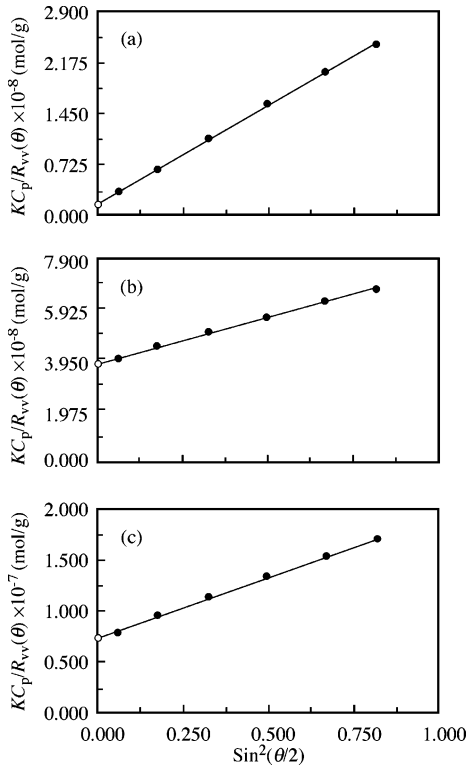

Figure 12. Angular dependence of $KC_p/R_{vv}(\theta)$ for aqueous solutions of PNIPAM$_{110}$-*b*-PNVP$_{53}$ (a), PNIPAM$_{110}$-*b*-PNVP$_{234}$ (b), and PNIPAM$_{76}$-*b*-PNVP$_{219}$ (c) at 60 °C.

This N_{agg} value for PNIPAM$_{110}$-*b*-PNVP$_{53}$ is obviously too large for a simple core−corona structure. Kim et al.[36,37] reported the formation of large aggregates of individual core−corona micelles formed from several kinds of amphiphilic diblock copolymers in water. Depending on the relative lengths of hydrophilic and hydrophobic blocks, a micelle core formed from hydrophobic blocks is not always completely protected from the exposure to the bulk water phase. Therefore, multicore structures may be formed by association of individual micelles, when the corona of the polymer micelle cannot completely prevent the hydrophobic interaction between the exposed hydrophobic cores of the micelles. Because the hydrophilic block length of PNIPAM$_{110}$-*b*-PNVP$_{53}$ is much shorter than those of the other two diblock copolymers, the individual simple core−corona micelles formed from PNIPAM$_{110}$-*b*-PNVP$_{53}$ may associate to form multi core intermicellar aggregates.

The ratio of $\langle R_g \rangle / \langle R_h \rangle$ is an important parameter that depends on the shape and polydispersity of the object. The theoretical value of $\langle R_g \rangle / \langle R_h \rangle$ for a homogeneous rigid sphere is 0.778, and it increases for a less dense structure and polydisperse solution.[38−41] The $\langle R_g \rangle / \langle R_h \rangle$ values for PNIPAM$_{110}$-*b*-PNVP$_{234}$ and PNIPAM$_{76}$-*b*-PNVP$_{219}$ micelles are 0.79 and 0.94, respectively, suggesting that these diblock copolymers form spherical micelles at 60 °C. On the other hand, $\langle R_g \rangle / \langle R_h \rangle$ for PNIPAM$_{110}$-*b*-PNVP$_{53}$ was found to be a much larger value of 2.7. Taken together with the N_{agg} data discussed above, it is suggested that PNIPAM$_{110}$-*b*-PNVP$_{53}$ forms elongated multicore aggregates formed by association of individual core−corona micelles.

Coating of Gold Nanoparticles with the Block Copolymer. It is known that PNVP can be attached to the surface of various metals.[15,16] Therefore, we looked into the capability of PNIPAM$_m$-*b*-PNVP$_n$ coating gold nanoparticles. We anticipate that, at room temperature, each of the polymer coated gold nanoparticles is separately dissolved in water without aggregation. However, at temperatures above LCST for the PNIPAM blocks, the gold

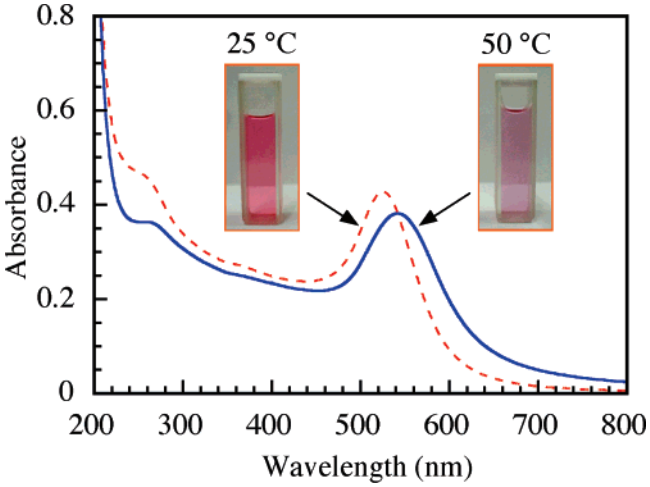

Figure 13. UV−vis absorption spectra for $PNIPAM_{110}$-*b*-$PNVP_{53}$ coated gold nanoparticles in 20 mM NaCl aqueous solutions at 25 (broken line) and 50 °C (solid line). Inserts show digital photographs of $PNIPAM_{110}$-*b*-$PNVP_{53}$ coated gold nanoparticles in 20 mM NaCl aqueous solutions at 25 and 50°.

nanoparticles may associate with each other due to the hydrophobic interactions between the dehydrated PNIPAM blocks.

Visible absorption spectra of the surface plasmon band for gold nanoparticles are known to be sensitive to the size of the gold nanoparticles. When gold nanoparticles are close to each other, the plasmon band around 520 nm shifts toward longer wavelengths.[42] Therefore, one can expect that the color of the polymer coated gold nanoparticles is pink at room temperature, and the color changes to bluish-purple at a higher temperature. To prepare polymer coated gold nanoparticles, we just mixed $PNIPAM_{110}$-*b*-$PNVP_{53}$ and gold nanoparticles in a 0.2 mM NaCl aqueous solution. Figure 13 compares UV−visible absorption spectra for the $PNIPAM_{110}$-*b*-$PNVP_{53}$ coated gold nanoparticles at 25 and 50 °C. At 25 °C, the surface plasmon band for the polymer coated gold nanoparticles can be observed at 525 nm, however at 50 °C, the absorption maximum shifts to a longer wavelength of 542 nm. The color of the polymer coated gold nanoparticles is pink at 25 °C. On the other hand, the pink color changes into bluish-purple at 50 °C. These observations indicate that heat-induced association of the $PNIPAM_{110}$-*b*-$PNVP_{53}$ coated gold nanoparticles can be controlled.

Conclusions

Polymerization of NVP, a nonconjugated monomer, can be controlled by TERP. The molecular weight distribution for PNVP prepared by TERP was narrower than that prepared by MADIX. Thermoresponsive diblock copolymers with different block lengths, $PNIPA_{110}$-*b*-$PNVP_{53}$, $PNIPAM_{110}$-*b*-$PNVP_{234}$, and $PNIPAM_{76}$-*b*-$PNVP_{219}$, were prepared by one pot synthesis using TERP. All the three block copolymers dissolve in water molecularly below T_a, however heat-induced micellization occurs above T_a due to the association of dehydrated PNIPAM blocks. T_a depends on the composition of the diblock copolymers. The diblock copolymer with longer PNVP and shorter PNIPAM blocks show a higher T_a while the diblock copolymer with shorter PNVP and longer PNIPAM blocks show a lower T_a. Light scattering data suggested that $PNIPAM_{110}$-*b*-$PNVP_{234}$ and $PNIPAM_{76}$-*b*-$PNVP_{219}$ form spherical core−corona micelles with N_{agg} = 808 and 298, respectively above T_a. In contrast, $PNIPAM_{110}$-*b*-$PNVP_{53}$ forms a much larger aggregate with N_{agg} = 27,000, which may be a multi core aggregate formed by the association of individual core−corona micelles.

Gold nanoparticles can be coated with $PNIPAM_{110}$-*b*-$PNVP_{53}$ because of coordinated interaction between the surface of gold nanoparticles and the PNVP blocks. The polymer coated gold nanoparticles indicate a temperature-dependent color change arising from a shift of visible absorption band. The maximum wavelength of the plasomon band for the polymer coated gold nanoparticles in a 20 mM NaCl aqueous solution at 25 °C shifted to a longer wavelength at 50 °C, suggesting that association behavior of the polymer coated gold nanoparticles can be controlled by temperature.

Acknowledgment. Financial supported by Grant-in-Aid for Scientific Research (No. 18750105) from the Japan Society for the Promotion of Science (JSPS) is gratefully acknowledged. We would also like to thank Otsuka Chemical and Nippon Shokubai for their gifts of BTEE and NVP, respectively.

Supporting Information Available: Figures showing a comparison of GPC elution profiles for PNVP prepared by TERP and MADIX, correlation functions, temperature dependence on light scattering intensity, angular dependence of QELS data, and d*n*/dC_p data. This material is available free of charge via the Internet at http://pubs.acs.org.

References and Notes

(1) Shi, L.; Chapman, T. M.; Beckman, E. J. *Macromolecules* **2003**, *36*, 2563−2567.
(2) Moad, G.; Rizzardo, E.; Thang, S. H. *Aust. J. Chem.* **2005**, *58*, 379−410.
(3) Wan, D.; Satoh, K.; Kamigaito, M.; Okamoto, Y. *Macromolecules* **2005**, *38*, 10397−10405.
(4) Charmot, D.; Corpart, P.; Adam, H.; Zard, S. Z.; Biadatti, T.; Bouhadir, G. *Macromol. Symp.* **2000**, *150*, 23−32.
(5) Chiefari, J.; Chong, Y. K.; Ercole, F.; Krstina, J.; Jeffery, J.; Le, T. P. T.; Mayadunne, R. T. A.; Meijs, G. F.; Moad, C. L.; Moad, G.; Rizzardo, E.; Thang, S. H. *Macromolecules* **1998**, *31*, 5559−5562.
(6) Yamago, S.; Ikeda, K.; Yoshida, J. *J. Am. Chem. Soc.* **2002**, *124*, 2874−2875.
(7) Yamago, S.; Ray, B.; Iida, K.; Yoshida, J.; Tada, T.; Yoshizawa, K.; Kwak, Y.; Goto, A.; Fukuda, T. *J. Am. Chem. Soc.* **2004**, *126*, 13908−13909.
(8) Yamago, S. *J. Polym. Sci., Part A: Polym. Chem.* **2006**, *44*, 1−12.
(9) Coote, M. L.; Radom, L. *J. Am. Chem. Soc.* **2003**, *125*, 1490−1491.
(10) Schinesser, C. H.; Smart, B. A. *Tetrahedron*, **1995**, *51*, 6051−6060.
(11) Yamago, S.; Miyazoe, H.; Goto, R.; Hashidume, M.; Sawazaki, T.; Yoshida, J. *J. Am. Chem. Soc.* **2001**, *123*, 3697−3705.
(12) Kwak, Y.; Tezuka, M.; Goto, A.; Fukuda, T.; Yamago, S. *Macromolecules* **2007**, *40*, 1881−1885.
(13) Wood, A. S. *Kirk-Othmer Encyclopedia of Chemical Technolgy*, 2nd ed.; Mcketta, J. J., Othmer, D. F., Standen, A., Eds.; Interscience: New York, 1970; pp 427−440.
(14) Haaf, F.; Sanner, A.; Straub, F. *Polym. J.* **1985**, *17*, 143−152.
(15) Einaga, H.; Harada, M. *Langmuir* **2005**, *21*, 2578−2584.
(16) Bian, C.-R.; Suzuki, S.; Asakura, K.; Ping, L.; Toshima, N. *J. Phys. Chem. B* **2002**, *106*, 8587−8598.
(17) McCormick, C. L., Ed. *Stimuli-Responsive Water Soluble and Amphiphilic Polymers*; ACS Symposium Series 780; The American Chemical Society: Washington, DC, 2001.
(18) Kikuchi, A.; Okano, T. *J. Controlled Release* **2005**, *101*, 69−84.
(19) Xiao, X.-C.; Chu, L.-Y.; Chen, W.-M.; Wang, S.; Xie, R. *Langmuir* **2004**, *20*, 5247−5253.
(20) Artoçaréna, M.; Heise, B.; Ishaya, Laschewsky, S. A. *J. Am. Chem. Soc.* **2002**, *124*, 3787−3793.
(21) Yusa, S.; Shimada, Y.; Mitsukami, Y.; Yamamoto, T.; Morishima, Y. *Macromolecules* **2004**, *37*, 7507−7513.
(22) Convertine, A. J.; Lokitz, B. S.; Vasileva, Y.; Myrick. L. J.; Scales, C. W.; Lowe, A. B.; McCormick, C. L. *Macromolecules* **2006**, *39*, 1724−1730.
(23) Yonezawa, T.; Toshima, N. In *Advanced Functional Molecules and Polymers*; Nalwa, H. S., Ed.; Gordon & Breach: Great Britain, Australia, 2001, Vol. 2, p 65.
(24) Tsunoyama, H.; Sakurai, H.; Negishi, Y.; Tsukuda, T. *J. Am. Chem. Soc.* **2005**, *127*, 9374−9375.
(25) Mirkin, C. A.; Letsinger, R. L.; Mucic, R. C.; Storhoff, J. J. *Nature (London)* **1996**, *382*, 607−609.

(26) Storhoff, J. J.; Lazarides, A. A.; Mucic, R. C.; Mirkin, C. A.; Letsinger, R. L.; Schatz, G. C. *J. Am. Chem. Soc.* **2000**, *122*, 4640−4650.
(27) Ishii, T.; Otsuka, H.; Kataoka, K.; Nagasaki, Y. *Langmuir* **2004**, *20*, 561−564.
(28) The toxicity of organotellurium compounds is not clear. They should be handled with care. See: Chasteen, T. G.; Bentley, R. *Chem. Rev.* **2003**, *103*, 1−26.
(29) Bouhadir, G.; Legrand, N.; Quiclet-Sire, B.; Zard, S. Z. *Tetrahedron Lett.* **1999**, *40*, 277−280.
(30) Satoh, N.; Hasegawa, H.; Tsujii, K.; Kimura, K. *J. Phys. Chem.* **1994**, *98*, 2143−2147.
(31) Jakes, J. *Collect. Czech. Chem. Commun.* **1995**, *60*, 1781−1797.
(32) Schillén, K.; Brown, W.; Johnsen, R. M. *Macromolecules* **1994**, *27*, 4825−4832.
(33) Brown, W.; Nicolai, T.; Hvidt, S.; Stepanek, P. *Macromolecules* **1990**, *23*, 357−359.
(34) Chu, B.; Wang, Z.; Yu, J. *Macromolecules* **1991**, *24*, 6832−6838.
(35) Pelton, R. H.; Chibante, P. *Colloids Surf.* **1986**, *20*, 247−256.
(36) Kim, C.; Lee, S. C.; Shin, J. H.; Yoon, J.-S.; Kwon, I. C.; Jeong, S. Y. *Macromolecules* **2000**, *33*, 7448−7452.
(37) Chang, Y.; Lee, S. C.; Kim, K. T.; Kim, C.; Reeves, S. D.; Allcock, H. R. *Macromolecules* **2001**, *34*, 269−274.
(38) Qin, A.; Tian, M.; Ramireddy, C.; Webber, S. E.; Munk, P.; Tuzar, Z. *Macromolecules* **1994**, *27*, 120−126.
(39) Nordmeier, E.; Lechner, M. D. *Polym. J.* **1989**, *21*, 623−632.
(40) Mössmer, S.; Spatz, J. P.; Möller, M.; Aberle, T.; Schmidt, J.; Burchard, W. *Macromolecules* **2000**, *33*, 4791−4798.
(41) Konishi, T.; Yoshizaki, T.; Yamakawa, H. *Macromolecules* **1991**, *24*, 5614−5622.
(42) Kreibig, U.; Vollmer, M. *Optical Properties of Metal Clusters*; Springer Series in Material Science 25; Springer-Verlag: Berlin, 1995.

MA070769X